

Supplementing the 2MRS survey: The 2MZoA catalogue

A.C. Schröder[1]

Max-Planck-Institut für extraterrestrische Physik, Gießenbachstraße 1, 85748 Garching, Germany, e-mail: anja@mpe.mpg.de

Received ...; accepted ...

ABSTRACT

We present a homogeneous catalogue of verified 2MASX galaxies in high extinction areas, which is complete to a Galactic extinction-corrected magnitude of $K_s^o \leq 11\overset{m}{.}75$. It covers the low Galactic latitudes ($|b| \leq 10\overset{\circ}{.}0$), called Zone of Avoidance (ZoA), and areas of high foreground extinctions ($E(B-V)> 0\overset{m}{.}95$) at higher latitudes. This catalogue supersedes the previously presented bright 2MZoA catalogue which was only complete to $K_s^o \leq 11\overset{m}{.}25$. It fully complements the 2MASS Redshift Survey (2MRS) galaxy catalogue, which has the same magnitude limit but excludes high extinction regions. The combination of the two catalogues, the extended 2MRS or e2MRS, is a uniquely whole sky redshift survey of galaxies and forms a sound basis for studies of large-scale structures, flow fields, and extinction across the ZoA.

The here presented catalogue comprises 6899 galaxies with 6757 galaxies at low latitudes and 142 galaxies in highly obscured high-latitude areas. The completion rate in redshifts is almost 75%. The catalogue is complete up to star density levels of at least $\log N_*/\mathrm{deg}^2 < 4.3$, but the completion rate of the fainter part is affected by foreground extinction at all levels. This can be rectified by using a diameter-dependent extinction correction, adding 605 highly obscured but apparently faint galaxies (with $K_s^o > 11\overset{m}{.}75$ and $K_s^{o,d} \leq 11\overset{m}{.}75$) to the sample. This extended sample shows good completion rates with extinction up to at least $A_K < 1\overset{m}{.}3$. Omission of such a diameter-dependent extinction correction may lead to a biased flow field even at intermediate extinction values as found in the 2MRS survey. As in our previous investigations, we recommend a correction factor $f = 0.86$ to be applied to the extinction maps, and we find it to be independent on Galactic longitudes or latitudes.

Key words. catalogues – galaxies; general – galaxies; photometry – infrared; galaxies

. Introduction

ur knowledge of the local Universe, that is, the local large scale tructures and related dynamics, is still incomplete due to the dif- culties in finding and studying galaxies near the Galactic plane, he so-called Zone of Avoidance (ZoA). Dust extinction as well s star crowding severely hinder both the identification of galax- es (where different wavelengths are affected by different biases, .g., Kraan-Korteweg & Lahav 2000 and references therein) as ell as follow-up observations to obtain, for example, redshifts e.g., Macri et al. 2019).

The ZoA is known to obscure and bisect major parts of dy- amically important structures such as the Perseus-Pisces Super- luster (Chamaraux et al. 1990; Focardi et al. 1984), the Great ttractor (Dressler et al. 1987; Kraan-Korteweg et al. 1996; Woudt et al. 2004), and the Local Void (Tully et al. 2019, 2008). ven to date, newly identified low-latitude structures are still eing discovered, for example the extended Vela supercluster Kraan-Korteweg et al. 2017) at $cz \sim 18,500\,\mathrm{km\,s^{-1}}$, contributing to the local bulk flow motion (e.g., Hudson et al. 2004; Springob et al. 2016).

While H I surveys are best in penetrating the foreground dust, they mainly trace filaments through gas-rich spiral galaxies. In contrast, NIR surveys serve better in getting a more comprehensive view of the local large-scale structures. Foreground extinction at these wavelengths is a lesser problem, and instead the detection of galaxies is more likely constrained by star crowding (e.g., Schröder et al. 2019, hereafter Paper I). The only truly all-sky NIR survey is the 2MASS (Two Micron All Sky Survey; Skrutskie et al. 2006) with a catalogue of extended sources, 2MASX (Jarrett 2004). A subset of this catalogue, restricted by Galactic latitude and foreground extinction, led to the 2MASS Redshift Survey (2MRS, Huchra et al. 2012).

2MASS is a comprehensive though shallow survey, but deeper NIR surveys, covering only the ZoA, exist, e.g., the UKIDSS GPS (Galactic Plane Survey; Lucas et al. 2008), the Vista VVV (VISTA Variables in the Vía Lactea; Minniti et al. 2010) as well as VVVX (the extended VVV; Saito et al. 2024), and the DECam Plane Survey (Schlafly et al. 2018). With their higher resolution they are ideal for detecting galaxies, but by-eye searches or even verification of automatically detected extended sources of such a data volume is not feasible anymore and one needs to rely on other methods, like machine learning (e.g., Alonso et al. 2025; Daza-Perilla et al. 2023).

To produce the extended 2MRS, e2MRS, which is the first nearly whole-sky redshift survey, our group has started to complement 2MRS by identifying 2MASX galaxies deep in the ZoA and measuring redshifts for them. As a pilot study, Paper I presents the 2MZoA catalogue of verified 2MASX galaxies down to an extinction-corrected magnitude limit of $K_s^o = 11\overset{m}{.}25$, which is complete up to star density levels of $\log N_*/\mathrm{deg}^2 < 4.5$, thus reducing the ZoA to $2.5-4\%$ of the whole sky. Kraan-Korteweg et al. (2018) observed useful candidates with the Nançay Radio Telescope (NRT), resulting in 232 detections. An optical spectrographic survey is still ongoing. Schröder et al. (2021, hereafter Paper II) has used this sample to investigate the Galactic foreground extinction and recommend the extinction map presented by Planck Collaboration et al. (2016) with a correction factor $f = 0.86\pm0.01$. In this paper, we present the extension of the 2MZoA catalogue down to an extinction-corrected magnitude limit of $K_s^o = 11\overset{m}{.}75$, so as to be fully complementary

Table 1. Object samples at different stages during extraction.

Sample	2MZoA		EBV	
	Paper I	this paper	Paper I	this paper
2MASX extraction	146 174	(same)	4248	(same)
all objects, bright sample	6913	6080	502	424
all objects, faint sample	–	3859	–	130
galaxies, bright sample	3671	3470	88	76
galaxy candidates, bright sample	4	3	0	0
galaxies, faint sample	–	3287	–	66
galaxy candidates, faint sample	–	6	–	0
galaxies total	3671	6757	88	142

to 2MRS. Obtaining the missing redshifts will be more difficult, especially since many of the faintest galaxies are too obscured for optical spectroscopy and will require (N)IR spectroscopy or H I observations.

This paper is organised as follows. In Sect. 2 we describe the sample, in Sect. 3 we present the catalogue and in Sect. 4 we investigate its properties. Section 5 discusses differences and commonalities with Paper I and of various subsamples. In Sect. 6 we revisit the investigation on Galactic foreground extinction from Paper II, using the new sample. Sect. 7 finishes with a summary. Online tables and some plots are presented in the appendix.

2. The sample

Details of the sample selection and extraction can be found in Paper I. For convenience, we give here a short summary and point out the differences due to the new selection criteria.

Our new magnitude limit is $K_s^o \leq 11\overset{m}{.}75$. Contrary to the 2MRS sample and our bright 2MZoA sample, we now choose to use a more suitable extinction map to correct for Galactic extinction, as investigated in Paper II. Instead of using the more common Schlegel et al. (1998) maps (hereafter SFD), we recommended the less biased Planck Collaboration et al. (2016) maps, which were reduced using the generalised needlet internal linear combination (GNILC) component-separation method, hereafter called GN extinction. Furthermore, we apply a correction factor $f = 0.86$ to the $E(B-V)$ values as also recommended in Paper II. For the 2MRS sample, the difference between the SFD and GN extinction corrections is considered negligible since they restrict their sample to areas where $E(B-V) < 1\overset{m}{.}0$. The difference to the bright 2MZoA sample will be more noticeable, with new galaxies being included in the sample and others excluded.

In addition, with more redshift information and deep NIR images that have become available since Paper I, some of the object classifications have changed. We will thus give a fully updated catalogue of all galaxies with $K_s^o \leq 11\overset{m}{.}75$ and include flags to indicate whether a galaxy is in the old and/or the new catalogue.

As in Paper I, we have compiled two subsamples:

ZOA sample: galaxies at $|b| \leq 10\overset{\circ}{.}0$ at all Galactic longitudes;

EBV sample: all objects at $|b| > 10\overset{\circ}{.}0$ with $E(B-V) > 0\overset{m}{.}95$. The limit refers to SFD extinctions as to be as close to the 2MRS selection as possible; the overlap range has been chosen to cover any small variations in the actual calculation of $E(B-V)$.

2.1. Sample extraction

From the online 2MASX catalogue[1], we extracted all sources with the above mentioned selection criteria as well as the default SQL constraints given in the webform. The resulting sample is the same as in Paper I, but we now apply the GN extinction correction to extract the magnitude-limited sample of objects, using the following extinction conversion factors (Fitzpatrick 1999): A_λ / A_B = 0.208, 0.128, 0.087 for J, H and K_s-band, repetitively. Table 1 lists the numbers of objects in the respective samples ZOA and EBV for the original catalogue (Paper I) and for the present catalogue. For better comparison we also give numbers for the bright sample ($K_s^o \leq 11\overset{m}{.}25$) and the faint sample ($11\overset{m}{.}25 < K_s^o \leq 11\overset{m}{.}75$) separately.

All 2MASX catalogue entries obeying the selection criteria have been inspected visually on optical and NIR images and given a flag according to the confidence we have that they are galaxies. Compared with Paper I, the availability of deep NIR survey images has increased[2], with 89% of the ZOA objects and 76% of the EBV objects now covered.

As in Paper I, we extracted redshift information from online data bases and literature, which also helped with the classification (see Appendix A for details). Finally, we visually estimated galaxy types regarding the presence or absence of a disc (mainly in preparation for H I follow-up observation); the B- and R-band images proved most useful for low-extinction galaxies, while the deep K-band images were most helpful in high-extinction areas. In addition to Paper I, we flag known and suspected active galaxies (AGNs) since these often have a redder colour. We have also revisited the extinction flag and reevaluated those for the bright sample.

As a result, we have a total of 6899 galaxies, with 6757 in the ZOA sample and 142 in the EBV sample. In addition, there are nine galaxy candidates, all in the ZOA sample. The differences to Paper I in the bright sample source numbers are mainly due to the here applied extinction correction factor (which reduces the extinction correction, resulting in fainter corrected magnitudes) and, to a smaller degree, due to differences between the SFD and GN extinction values.

2.2. Subsamples and supplementary samples

In the catalogue, we give flags for various sample definitions for convenience. As already indicated in Table 1, we can define a bright and a full sample (with $K_s^o \leq 11\overset{m}{.}25$ and $K_s^o \leq 11\overset{m}{.}75$, respectively). For easier comparison with Paper I, we give an 'original sample' flag based on SFD extinction correction with no correction factor (note that the number of galaxies in this sample still differs from Paper I due to changes in galaxy class settings). We also give a flag for the full sample but with no correction factor applied to the $E(B-V)$ values, which makes it easier to investigate this factor further if there is a need.

We list the sample flags with their definitions as well as the numbers of objects and of galaxies in Table 2. Note that the sample flags do not distinguish between the ZOA and EBV sample since these can be simply selected by Galactic latitude.

As mentioned in Paper I, the isophotal diameter of a galaxy is also affected by extinction, and an additional, diameter-dependent, extinction correction should be applied. This correc-

[1] See the 2MASS All-Sky Extended Source Catalog (XSC) as found online at http://irsa.ipac.caltech.edu/cgi-bin/Gator/nph-dd

[2] e.g., UHS (UKIRT Hemisphere Survey, Dye et al. 2018) and VVVX (Saito et al. 2024) survey images have become available in the meantime.

Table 2. Various sample flags

Sample	Selection	Flag	ZOA			EBV		Total	
			Objects	Galaxies	Cand.	Objects	Galaxies	Objects	Galaxies
Full sample S	$K_s^o \leq 11\overset{\text{m}}{.}75$, GN, f = 0.86	f_{sam}	9939	6757	9	554	142	10493	6899
Bright (original) sample, Paper I	$K_s^o \leq 11\overset{\text{m}}{.}25$, SFD, f = 1.0	f_{orig}	6913	3693	3	502	89	7415	3782
Bright sample, this paper	$K_s^o \leq 11\overset{\text{m}}{.}25$, GN, f = 0.86	f_{br}	6080	3470	3	424	76	6504	3546
Full sample, f = 1.0	$K_s^o \leq 11\overset{\text{m}}{.}75$, GN, f = 1.0	f_{no-f}	10447	7099	14	585	152	11032	7251
With diameter-dependent extinction corrections:									
Extended sample S*e*	$K_s^{o,d} \leq 11\overset{\text{m}}{.}75$, GN, f = 0.86	f_{ext}	10960	7344	16	616	160	11576	7504
Bright extended sample, Paper I	$K_s^{o,d} \leq 11\overset{\text{m}}{.}25$, SFD, f = 0.83	$f_{ext-orig}$	7158	3734	5	515	90	7673	3824

tion, however, has large uncertainties and is best applied to the individual galaxy photometry by extrapolating the radial brightness curves (Riad et al. 2010). We therefore do not use it in our recommended sample. Instead, we have compiled an extended sample based on these corrections, which will help to understand the effects of applying such a correction on sample size and characteristics. We give two such sample flags: one is based on the faint limit $K_s^{o,d} \leq 11\overset{\text{m}}{.}75$, with the GN extinction correction and a factor 0.86 applied, the other refers to the sample presented in Paper I and is based on the SFD extinctions ($K_s^{o,d} \leq 11\overset{\text{m}}{.}25$), with a correction factor $f = 0.83$ applied.

3. The catalogue

The catalogue with a total of 10960 ZOA and 616 EBV objects is available online at CDS; a few example rows are listed in Table A.1 in the appendix. It supersedes the catalogues given in Paper I. The table comes in two sections: (a) full sample as per our selection criteria, and (b) supplementary sample for objects that obey the limit $K_s^{o,d} \leq 11\overset{\text{m}}{.}75$ but not $K_s^o \leq 11\overset{\text{m}}{.}75$ when a diameter-dependent extinction correction is applied[3]. Columns are the same as in Paper I except for a different suite of sample flags, listed in Col. 7, and an updated object flag in Col 6, which now includes an indicator for AGNs. We have also added the best velocity measurement found in the literature, and include detailed flags separately for optical and H I velocities in Col. 10.

The columns are as follows:

Col. 1: ID: 2MASX catalogue identification number (based on J2000.0 coordinates).

Col. 2a and 2b: Galactic coordinates: longitude l and latitude b, in degrees.

Col. 3: Extinction: $E(B-V)$ value derived from the GNILC Planck maps (Planck Collaboration et al. 2016), in magnitudes.

Col. 4: Object class: 1 = obvious galaxy, 2 = galaxy, 3 = probable galaxy, 4 = possible galaxy, 5 = unknown, 6 = lower likelihood for galaxy, 7 = unlikely galaxy, 8 = no galaxy, 9 = obviously not a galaxy.

Col. 5: Object offset flag: 'o' stands for coordinates that are offset from the centre of the object, and 'e' stands for a detection near the edge of an image (at an offset position from the object centre; the properly centred object is detected on the adjacent image).

Col. 6: Object flag: 'p' stands for Planetary Nebula (PN), 'q' indicates a QSO/AGN, and 'b' stands for blazar; tentative classifications are indicated by a question mark.

Col. 7: Sample flags in the following order:

(a) f_{gal}: Galaxy flag: 'g' denotes a galaxy (object classes 1 – 4), and 'p' stands for galaxy candidates (class 5);
(b) f_{sam}: Full sample ($K_s^o \leq 11\overset{\text{m}}{.}75$, GN extinction correction, $f = 0.86$);
(c) f_{orig}: Bright sample as in Paper I ($K_s^o \leq 11\overset{\text{m}}{.}25$, SFD extinction correction, no correction factor);
(d) f_{br}: Bright sample, this paper, for comparison with Paper I ($K_s^o \leq 11\overset{\text{m}}{.}25$, GN extinction correction, $f = 0.86$);
(e) f_{no-f} : Full sample with no correction factor applied ($K_s^o \leq 11\overset{\text{m}}{.}75$, GN extinction correction, $f = 1.0$);
(f) f_{ext}: Extended sample, with diameter-dependent extinction correction applied ($K_s^{o,d} \leq 11\overset{\text{m}}{.}75$, GN extinction correction, $f = 0.86$);
(g) $f_{ext-orig}$: Extended sample as in Paper I, with diameter-dependent extinction correction ($K_s^{o,d} \leq 11\overset{\text{m}}{.}75$, SFD extinction correction, $f = 0.83$).

Col. 8: Galaxy disc type: 'D1' means an obviously visible disc and/or spiral arms, 'D2' stands for a noticeable disc, 'D3' for a possible disc, and 'D4' stands for no disc noticeable. Where it was not possible to tell (likely due to adjacent or superimposed stars or very high extinction) we give a flag 'n'.

Col. 9: 2MRS flags: 'c' stands for an entry in the main catalogue, and 'e' for the extra catalogue (that is, outside the 2MRS selection criteria) . For the sub-catalogues[4] we give: 'cf' for an entry in the flg catalogue (affected by nearby stars, but not severely), 'cp' for an entry in the flr catalogue (severely affected by nearby stars), 'ca' and 'ea' are objects that have been reprocessed and are both in the rep as well as add catalogues (in the latter case with new IDs and photometry, not listed by us), 'cr' and 'er' are objects rejected as galaxies and which can be found in the rej catalogues, 'cn' and 'en' are objects that have no redshifts yet and are listed in the nocz catalogues.

Cols. 10a – 10c: Velocity flags 'vo', 'vh' and 'vtot': 'o' stands for an optical measurement and 'h' for H I velocity; a colon indicates an uncertain measurement and a question mark stands for a questionable measurement, object ID or target (in particular for H I: a radio telescope's large beam size may include nearby galaxies), or an uncertain detection (often with a low signal-to-noise ratio); 'g' indicates a velocity measurement of a Galactic source[5]. Square brackets in Cols. 10a and 10b indicate a non-accepted velocity (due to questionable ID or measurement), and normal brackets in Col. 10c indicate not yet published measurements. In a few cases, though published values exist we prefer unpublished measurements (e.g., when they have better errors).

[3] A third section comprises 12 additional galaxies neither included in the full nor in the supplementary sample but which have $K_s^o \leq 11\overset{\text{m}}{.}75$ if no correction factor is applied to the extinction; we only list these for the comparison of samples, they are not used elsewhere.

[4] for a detailed description see http://tdc-www.harvard.edu/2mrs/2mrs_readme.html

[5] Though only objects flagged as galaxies (cf. Col. 7a) have velocity entries listed in the table, there are a few uncertain galaxies with questionable velocity measurements.

Col. 11: Deep NIR image flag: 'U' indicates a UKIDSS image for this object, 'H' stands for a UHS, and 'V' stands for VISTA.
Col. 12: Photometry flag: 'O' indicates off-centre coordinates (cf. Col. 5), 'A', 'P' and 'F' refer to the respective 2MRS flag (cf. Col. 9), and 'C' denotes improved photometry exists in John Huchra's original list (see Paper I for details).
Col. 13: Extinction flag (see Paper I): 'e' stands for a likely wrong extinction value, either due to small-scale variations or a non-removed FIR point source, 'e?' denotes a possible wrong extinction value. Note that these have been updated since Paper I.
Col. 14: 2MASX magnitude K_{20}: isophotal K_s-band magnitude measured within the K_s-band 20 mag arcsec^{-2} isophotal elliptical aperture (in magnitudes).
Cols. 15 and 16: 2MASX colours $(H-K_s)$ and $(J-K_s)$: isophotal colours measured within the K_s-band 20 mag arcsec^{-2} isophotal elliptical aperture (in magnitudes).
Col. 17: 2MASX flag *vc*: the visual verification score of a source.
Col.18: 2MASX object size a: the major diameter of the object, which is twice the 2MASX K_s-band 20 mag arcsec^{-2} isophotal elliptical aperture semi-major axis `r_k20fe` (in arcseconds).
Col. 19: 2MASX axis ratio b/a: minor-to-major axis ratio fit to the 3σ super-co-added isophote, `sup_ba`. Single-precision entries are given in cases where the 2MASX parameter `sup_ba` is not determined; these values were estimated from the axial ratios available in the different passbands.
Col. 20: 2MASX stellar density: co-added logarithm of the number of stars (K_s< 14 mag) per square degree around the object.
Cols. 21 – 23: Magnitude K_s^o and colours $(H-K_s)^o$ and $(J-K_s)^o$ corrected for foreground extinction (Col. 3) using a correction factor 0.86 (in magnitudes).
Col. 24: Extinction in the K_s-band A_K: calculated from $E(B-V)$ in Col. 3 and applying a correction factor of 0.86 (in magnitudes).
Col. 25: Extinction corrected major diameter a^d according to Riad et al. (2010) using $E(B-V)$ from Col. 4 with the correction factor 0.86; only given for objects classified as galaxies (in arcseconds).
Col. 26: Extinction corrected magnitude $K_s^{o,d}$ corrected according to Riad et al. (2010) using $E(B-V)$ from Col. 3 with the correction factor 0.86; only given for objects classified as galaxies (in magnitudes).
Cols. 27 and 28: Adopted radial, heliocentric velocity with error and reference according to the vtot flag in Col. 10c. If the measurement is not yet published, we quote a token reference and do not give the velocity here.

4. Properties of the catalogue

We have thoroughly discussed the properties of the bright 2MZoA catalogue in Paper I, and most of it also applies to the full sample. In the following, we show some updated plots and statistics. A sky map with the distribution of the samples are shown in the appendix; it is not qualitatively different from the maps shown in Paper I.

Figure 1 shows the colour–colour plot with objects classified as galaxies in black and non-galaxies in yellow; the few galaxy candidates (objects of unknown classification, class 5) are shown in green. Clearly offset in $(H-K_s)^o$ colour are PNe, which are shown as blue dots (where open circles indicate possible PNe).

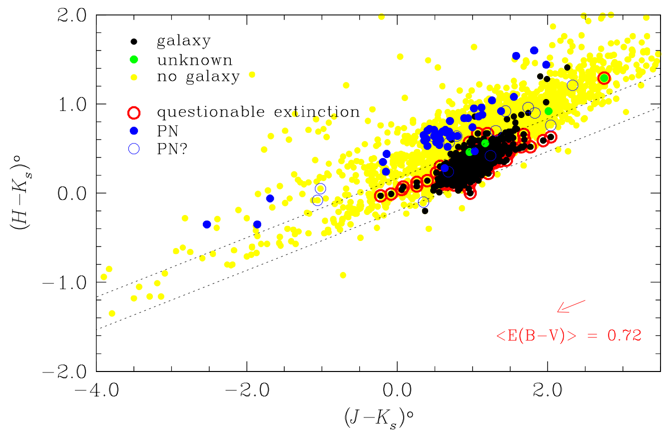

Fig. 1. 2MASS extinction-corrected colour–colour plot, $(H-K_s)^o$ versus $(J-K_s)^o$. A reddening vector, representing the mean of the sample shown, is indicated by a red arrow in the bottom right corner. The reddening path for objects within the intrinsic colour range of galaxies is indicated with two parallel dashed lines.

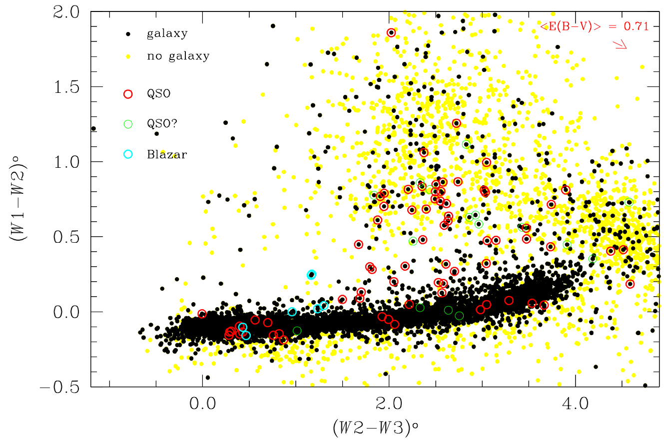

Fig. 2. WISE extinction-corrected colour–colour plot, $(W1-W2)^o$ versus $(W2-W3)^o$, for the full sample. A reddening vector, representing the mean of the sample shown, is indicated by a red arrow in the top right corner. Open circles mark active galaxies as labelled.

The reddening path for the intrinsic colour range occupied by the bulk of the galaxies is shown by the two dashed lines. Galaxies with wrong Galactic extinction values scatter along this path. This is confirmed by the distribution of the red circles which mark galaxies where we stated a questionable extinction based on visually obvious variations across the images (extinction flag *e*). Galaxies lying outside the reddening path are likely to be affected by starlight in the photometry aperture.

For the WISE colour–colour plot (Fig. 2) we use the aperture 1 (5.″5) magnitudes of the ALLWISE catalogue, corrected for foreground extinction, as in Paper I. Spiral galaxies are located more to the right, and ellipticals are predominantly found to the left (see Figure 26 in Jarrett et al. 2011), while active and intensely star forming galaxies are separated in $(W1-W2)$, top. We marked all AGNs listed in the literature with red circles and blazars with cyan circles; possible AGNs (based on their colour and visual appearance) are marked with green circles.

The completeness of a sample of galaxies can be shown in various ways. Figure 3 shows histograms of source counts as a function of Galactic latitude and longitude. While the galaxy counts (red) show a small dip near the Galactic plane (Panel (a)), the distribution of all sources (in blue) shows a clear peak, em-

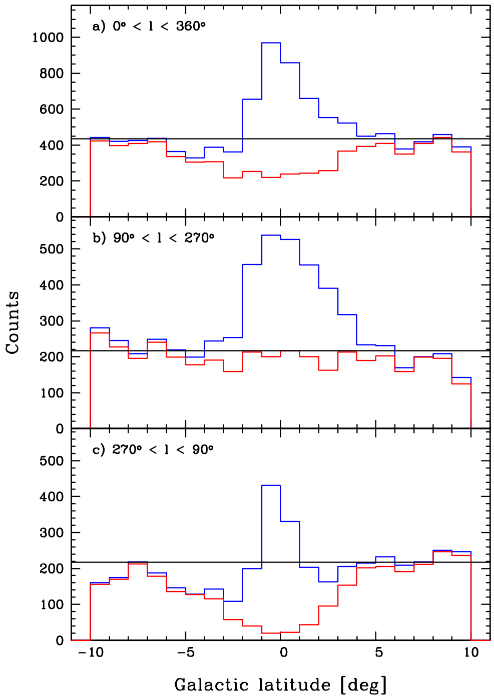

Fig. 3. Histograms of objects in the ZOA sample as a function of Galactic latitude for all objects (blue) and for galaxies only (red). The black line represents the average 2MASX galaxy count outside the ZoA. Panel (a): for all Galactic longitudes; panel (b) for the semi-circle towards the anti-centre region; panel (c) for the semi-circle towards the bulge.

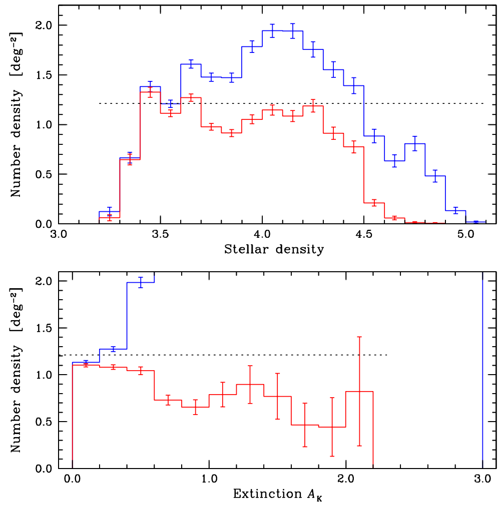

Fig. 4. Histograms of the number density of all ZOA sample objects (blue) and galaxies only (red) as a function of stellar density (top panel) and Galactic extinction A_K (bottom panel; only regions with $\log N_*/\mathrm{deg}^2 \leq 4.5$ were used). The error bars indicate Poissonian errors per bin. The black dotted lines represent the average 2MASX bright galaxy number density outside of the ZoA.

phasising the need for visual inspection to identify non-galaxian extended objects in the 2MASX catalogue for the inner ZoA ($|b| < 5°$). For comparison, the black line represents the average galaxy density outside of the ZoA, which is 1.212 galaxies/sq.deg (black line) based on source counts of the 2MASX catalogue with $|b| > 30°$ and $K_{20} \leq 11\overset{\mathrm{m}}{.}75$. Panels (b) and (c) show the semi-circles towards the anti-centre and the Galactic bulge, respectively. The dip in galaxy counts disappears in the anti-centre direction but is greatly pronounced towards the Galactic bulge. As already noted in Paper I, the dip towards the Galactic Bulge indicates a breakdown in galaxy recognition of the 2MASX survey mainly due to star crowding.

We can also show completeness levels as a function of stellar densities and extinction, see Fig. 4 top and bottom panel, respectively. For the extinction plot we only used areas with stellar densities $\log N_*/\mathrm{deg}^2 < 4.5$ (to avoid a selection bias since both high extinction and high stellar density occur in similar areas). The number densities are highly affected by low number statistics for $A_K \gtrsim 1\overset{\mathrm{m}}{.}0$. Due to the small area covered by our sample, the numbers are also subject to cosmic variance. However, we can make two broad statements: Extinction seems to affect galaxy counts at all levels, and the effect of stellar density is negligible up to $\log N_*/\mathrm{deg}^2 \sim 4.3$ and becomes severe at $\log N_*/\mathrm{deg}^2 > 4.5$.

Table 3 gives the statistics on some of the parameters in the ZOA and EBV catalogues. For better comparison, we give percentages with respect to all galaxies in the respective sample, with the total numbers listed at the bottom. Regarding the disc parameter, we find that over 80% of all galaxies show a disc, while only around 4% have no indication of one. Extinction flags were set for ~20% of galaxies in the ZOA sample, with a much higher fraction of ~65% for the EBV sample. The latter is expected since the EBV sample covers only high extinction areas.

As to redshift information, more than 70% of the sample galaxies have redshift measurements, the majority of which are optical. We distinguish between optical and H I measurements, and also whether the velocity information has been published[6] (v_{lit}). We separately list cases where it appears questionable that the measured redshift belongs to the targeted galaxy (indicated with a question mark). This mainly concerns H I measurements where the often very large beam size can include other galaxies close by. Though we give such velocities in our catalogue,

Table 3. Statistics on some parameters for both samples.

Param	meaning	ZOA sample [%]	EBV sample [%]
Disc class:			
D1	obvious disc	55.1	54.2
D2	disc	25.4	29.6
D3	possible disc	13.6	9.2
D4	no disc	4.3	3.5
n	unable to tell	0.7	0.7
Extinction flag:			
e	likely wrong ext	11.7	44.4
e?	possibly wrong ext	9.6	19.0
Velocities:			
v_{tot}	adopted (opt or HI)	72.4	76.7
v_{op}	opt	64.0	70.4
v_{op}?	uncertain ID	0.3	1.4
v_{hi}	H I	17.0	21.8
v_{hi}?	uncertain ID	0.3	0.7
$v_{\mathrm{lit-op}}$	published	58.0	68.3
$v_{\mathrm{lit-op}}$?	uncertain ID	0.5	7.0
$v_{\mathrm{lit-hi}}$	published	16.1	17.6
$v_{\mathrm{lit-hi}}$?	uncertain ID	1.2	0.7
2MRS	main catalogue	49.8	16.2
2MRS	extra catalogue	10.8	54.2
Total *N*		6757	142

[6] Some of the redshift measurements we use in our catalogue are work in progress and were obtained by members of our group and collaborators, see Schröder et al. (2021) for details.

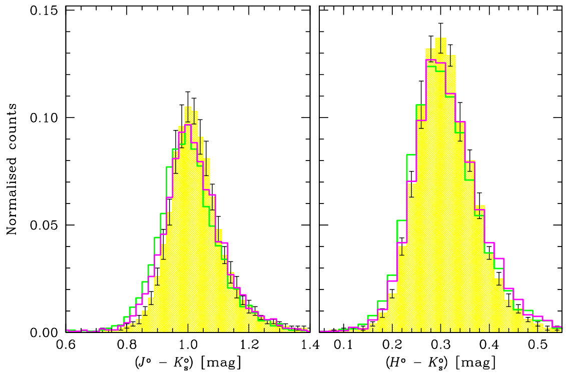

Fig. 5. Normalised histograms of 2MASX colours $(J - K_s)^o$ (left) and $(H - K_s)^o$ (right). Green histograms are the full sample and the magenta histograms show colours corrected for stellar densities. the yellow-filled histograms represent the average high Galactic latitude sample.

they have been flagged in Col. 10c with a question mark and are ignored in our analysis.

We have also flagged all objects that appear in the 2MRS catalogues (Huchra et al. 2012, Macri et al. 2019), though the percentages given here relate only to objects classified by us as galaxies. Furthermore, we have noted but not extracted photometric redshift information in the literature[7]. Since photometric redshifts have large uncertainties (and can be affected by stars in the aperture), we do not find them useful for our, predominantly local, sample. Finally, we noted a number of possible H I detections, which need confirmation before we can make use of them.

Figure 5 shows the histograms for the $(J-K_s)^o$ and $(H-K_s)^o$ colours (green lines). In Paper I we had found that there is a dependence on stellar density. We re-analysed the relationship for the new sample and found slightly improved dependencies:

$$(J - K_s)^o = (-0.064 \pm 0.007) \cdot \log N_*/\mathrm{deg}^2 + (1.244 \pm 0.027)$$

and

$$(H - K_s)^o = (-0.039 \pm 0.005) \cdot \log N_*/\mathrm{deg}^2 + (0.453 \pm 0.020).$$

The magenta-coloured histogram shows the accordingly corrected colours, and Table 4 gives the statistics of the colours with and without the correction. As in Paper I, we also show the histograms for galaxies outside the ZoA for comparison (yellow). Contrary to Paper I, we choose a higher latitude cut-off to make sure that extinction will not affect the (uncorrected) colours. With cuts at $|b| > 30°$ and $K_s < 11\overset{m}{.}75$, the high-latitude sample comprises 25 007 galaxies. As described in Paper I in more detail, we formed 16 subsamples containing each about 3000 galaxies to test for cosmic variance. The yellow histograms show the mean normalised counts with error bars based on the standard deviation of the 16 subsamples. The mean as well as the range of values for the 16 high-latitude subsamples are also given in Table 4. Since colours are affected by *k*-correction (noticeable as an extended red tail in the histograms), we prefer the median to the mean. There is good agreement between the high and low latitude samples if we apply the stellar density correction to our sample.

5. Sample comparisons

There are two major differences to Paper I:

1. As explained above, we use an improved extinction correction, which changes the composition of the sample for $K_s^o \leq 11\overset{m}{.}25$. In addition, with new deep NIR images and velocity information, some objects have a changed object class and have thus entered or left the bright galaxy sample.
2. By extending the magnitude limit from $11\overset{m}{.}25$ to $11\overset{m}{.}75$, the qualitative composition of the sample likely has changed since fainter galaxies are either smaller or more distant galaxies.

5.1. Comparison with Paper I

We can make a direct comparison with Paper I by applying the same magnitude limit $11\overset{m}{.}25$ to our here presented sample. First of all, the new sample is smaller since we also apply a correction factor smaller than one to the extinction values, resulting in fainter magnitudes, which affects the sample size. For clarity, we have also compared the effects of applying the SFD corrections (with and without a correction factor) instead of the GN extinction. The top section of Table 5 gives the various sample sizes.

While for each galaxy the GN extinction value may be smaller or larger than the SFD value, the overall effect on the sample is that we lose more objects than we gain. However, this seems to be only the case for the non-galaxies ($\Delta N = 405$ and 452 for the ZOA sample, depending on whether f was applied or not, respectively), while the differences in the galaxy samples are negligible ($\Delta N = -37$ and -10, respectively). We therefore do not expect (and have not found) any qualitative differences with the discussion in Paper I regarding the bright galaxy sample.

5.2. Bright versus faint

To investigate qualitative differences between bright and faint galaxies, we have divided our sample into the three subsamples bright (S1), medium (S2) and faint (S3), with $K_s^o \leq 11\overset{m}{.}25$, $11\overset{m}{.}25 < K_s^o \leq 11\overset{m}{.}50$ and $11\overset{m}{.}50 < K_s^o \leq 11\overset{m}{.}75$, respectively. Sample sizes are given in the second part of Table 5.

First of all, we show the distribution of the three subsamples across Galactic latitudes in Fig. 6 for all sources (left panel), galaxies (middle panel) and the ratio of galaxies versus all sources (right panel). While the dip in galaxy numbers seen in Fig. 3 around the Galactic plane persists (and varies similarly with longitude, not shown), only the S1 sample (red) shows a clear peak of non-galaxies near the plane. To investigate this further, we show the K_s^o band histogram in Fig. 7 (left panel) for non-galaxies in black and galaxies in red. While the galaxies show the typical exponential luminosity function, the number counts of non-galaxies increases much slower (almost but not quite linearly). It should be noted that the non-galaxies are mainly Galactic nebulae or parts thereof, with some artefacts and stars or batches of faint stars added to the mix. Due to their size and the overestimation of foreground extinction, the detections of the nebulae are usually bright, and it is therefore obvious that the fainter samples show much less contamination. To emphasise this, we show the histogram of diameters (right hand panel in Fig. 7). At large diameters the non-galaxies dominate as expected. Non-galaxies also dominate at the smallest diameters, which is likely due to the spurious detection of stars.

Figure 8 compares the samples regarding stellar density (left panel) and extinction (right panel). All three samples show stable number densities for stellar densities of $\log N_*/\mathrm{deg}^2 \geq 3.4$, the sharp cut-off at $\log N_*/\mathrm{deg}^2 \geq 4.5$ known from Paper I (and here visible for S1) is less pronounced for the fainter samples with a reduced limit of $\log N_*/\mathrm{deg}^2 \sim 4.4$, indicating that stellar

[7] The majority of which can be found in the 2MASS Photometric Redshift catalogue by Bilicki et al. (2014).

Table 4. Statistics on 2MASX colours of various samples

Sample	$(J - K_s)$					$(H - K_s)$				
	N	median [mag]	mean [mag]	error [mag]	standard deviation [mag]	N	median [mag]	mean [mag]	error [mag]	standard deviation [mag]
Colour^{o}	4932	0.990	1.001	0.002	0.11	5000	0.300	0.306	0.001	0.08
Colour^{o,c}	4904	1.011	1.019	0.002	0.11	4972	0.309	0.318	0.001	0.08
Colour (high-lat)	24 966	1.018	1.030	0.001	0.13	24 967	0.306	0.315	0.001	0.09
Colour (high-lat)	2952 – 3290	1.009 – 1.027	1.019 – 1.044	0.001 – 0.002	0.10 – 0.20	2952 – 3289	0.301 – 0.311	0.308 – 0.323	0.001 – 0.002	0.07 – 0.13

Table 5. Various samples with different K^o_s band limits.

Sample	Source of extinction	f	ZOA sample N_{obj}	N_{gal}	EBV sample N_{obj}	N_{gal}
Bright samples ($K^o_s \leq 11\overset{m}{.}25$):						
Paper I	SFD	1.0	6913	3693	502	89
This paper (S1)	GN	0.86	6080	3470	424	76
– Variation A	SFD	0.83	6448	3433	465	78
– Variation B	SFD	1.0	6835	3645	492	88
– Variation C	GN	1.0	6393	3655	441	78
Fainter samples:						
S2 ($11\overset{m}{.}25 < K^o_s \leq 11\overset{m}{.}50$)	GN	0.86	1577	1305	53	20
S3 ($11\overset{m}{.}50 < K^o_s \leq 11\overset{m}{.}75$)	GN	0.86	2282	1982	77	46
Supplementary sample:						
S+ ($K^o_s > 11\overset{m}{.}75$, $K^{o,d}_s \leq 11\overset{m}{.}75$)	GN	0.86	1021	587	62	18

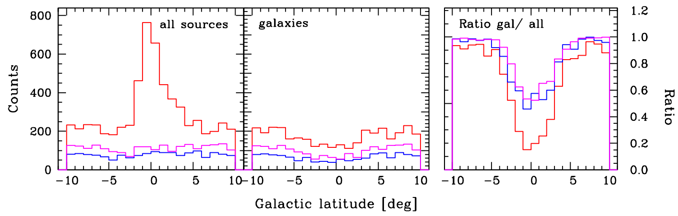

Fig. 6. Histograms of objects in the ZOA samples with Galactic latitude: all objects (left), galaxies (middle) and the fraction of galaxies (right). S1 is shown in red, S2 in blue and S3 in magenta).

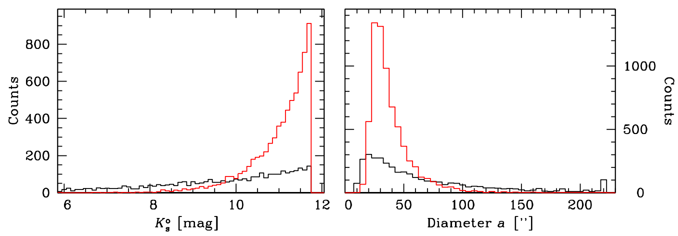

Fig. 7. Histograms of objects in the full sample: non-galaxies are in black and galaxies in red. Left: As a function of extinction-corrected K^o_s band magnitude; right: as a function of diameter in arcseconds.

densities affect more the detection of smaller and fainter galaxies. The extinction also affects more strongly the two fainter samples. Due to the limit in extinction-corrected magnitude, the maximum A_K value drops from $2\overset{m}{.}1$ to $1\overset{m}{.}7$ to $1\overset{m}{.}3$, respectively. The faintest sample S3 (magenta) shows a decrease even in the first three bins ($A_K < 0\overset{m}{.}6$) and both S2 and S3 show a gradual decrease beyond $A_K = 0\overset{m}{.}6$. We conclude that the faintest sample is not complete at any extinction level.

Statistics of the parameters disc class, extinction flag and availability of redshift measurement information are presented in Table 6, similarly to Table 3. While the disc class parameter shows the increasing difficulties to classify fainter (and smaller) galaxies, the determination of the extinction flag is

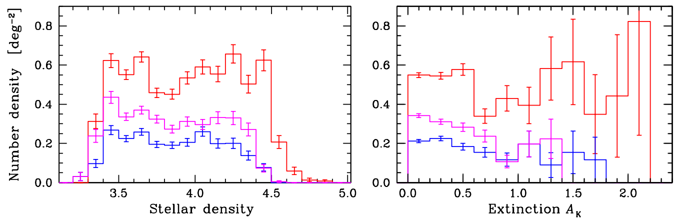

Fig. 8. Same as Fig. 4 for the galaxies in the subsamples S1 (red), S2 (blue) and S3 (magenta).

Table 6. Statistics on some parameters for the subsamples.

Param	ZOA samples S1 [%]	S2 [%]	S3 [%]	S+ [%]	EBV samples S1 [%]	S2 [%]	S3 [%]	S+ [%]
Disc class:								
D1	59.0	54.8	48.4	43.3	55	50	54	61
D2	21.8	26.0	31.3	28.4	33	35	22	11
D3	11.0	15.1	17.1	19.8	5	10	15	17
D4	6.1	2.9	2.2	3.7	3	5	4	11
n	0.3	1.1	1.1	4.8	1	0	0	0
Extinction flag:								
e	12.2	11.2	11.3	20.4	38	45	54	44
e?	9.2	9.0	10.2	19.8	17	20	22	28
Velocities:								
v_{tot}	85.5	65.0	54.7	14.8	93	75	50	22
v_{op}	72.9	59.0	51.8	13.3	86	75	44	17
v_{op}?	0.4	0.3	0.3	0	0	5	2	0
v_{hi}	26.6	10.7	4.6	1.9	30	20	9	6
v_{hi}?	0.3	0.5	0.3	0.2	0	0	2	0
v_{lit-op}	62.7	55.1	51.7	13.3	83	70	44	17
v_{lit-op}?	0.7	0.5	0.3	0.2	4	10	11	6
v_{lit-hi}	25.0	10.3	4.6	1.9	26	15	4	6
v_{lit-hi}?	1.4	0.9	0.7	0.2	0	0	2	0
2MRS main	49.3	50.2	50.6	11.4	20	5	15	17
2MRS extra	17.4	6.1	2.6	1.7	66	65	30	0
Total N	3470	1305	1982	587	76	20	46	18

independent of the kind of detected galaxy. There is also a marked (and expected) decrease in redshift measurements for the fainter samples, especially in H I measurements. This is partly because mostly bright and large galaxies are targeted in H I surveys. In addition, the sensitivity decreases rapidly with distance so that most blind H I surveys do not go much beyond $v = 10\,000\,\mathrm{km\,s^{-1}}$. However, this will change with the new generation of radio telescopes like MeerKAT, ASKAP and, eventually, the SKA.

Representation in the 2MRS catalogue is stable across all samples as expected since we choose the same magnitude limit. The inclusion in the 2MRS extra catalogue decreases for the fainter samples since galaxies were not systematically included in this catalogue but only through availability of redshift measurements in the literature.

Table 7. Statistics on 2MASX colours of various samples.

Sample	$(J - K_s)$					$(H - K_s)$				
	N	median [mag]	mean [mag]	error [mag]	standard deviation [mag]	N	median [mag]	mean [mag]	error [mag]	standard deviation [mag]
Colour^{o} S1	2547	0.980	0.985	0.002	0.10	2582	0.290	0.292	0.001	0.07
Colour^{o,c} S1	2520	0.994	1.004	0.002	0.10	2555	0.298	0.305	0.001	0.07
Colour (high-lat) S1	12 607	1.000	1.013	0.001	0.13	12 609	0.293	0.302	0.001	0.09
Colour (high-lat) S1	1444 – 1719	0.991 – 1.011	1.002 – 1.028	0.002 – 0.004	0.10 – 0.23	1441 – 1718	0.289 – 0.298	0.295 – 0.310	0.001 – 0.003	0.06 – 0.14
Colour^{o} S2	965	1.010	1.011	0.004	0.11	976	0.310	0.314	0.002	0.08
Colour^{o,c} S2	965	1.025	1.028	0.004	0.11	976	0.320	0.325	0.002	0.08
Colour (high-lat) S2	5156	1.030	1.042	0.002	0.12	5156	0.315	0.322	0.001	0.08
Colour (high-lat) S2	601 – 697	1.021 – 1.041	1.031 – 1.058	0.003 – 0.007	0.09 – 0.20	601 – 697	0.310 – 0.321	0.315 – 0.332	0.001 – 0.002	0.06 – 0.12
Colour^{o} S3	1420	1.020	1.025	0.003	0.12	1442	0.320	0.325	0.002	0.10
Colour^{o,c} S3	1419	1.034	1.041	0.003	0.12	1441	0.327	0.336	0.002	0.09
Colour (high-lat) S3	7170	1.042	1.052	0.001	0.11	7169	0.325	0.332	0.001	0.08
Colour (high-lat) S3	835 – 949	1.027 – 1.054	1.042 – 1.066	0.002 – 0.004	0.09 – 0.14	835 – 950	0.317 – 0.333	0.324 – 0.340	0.002 – 0.003	0.07 – 0.10

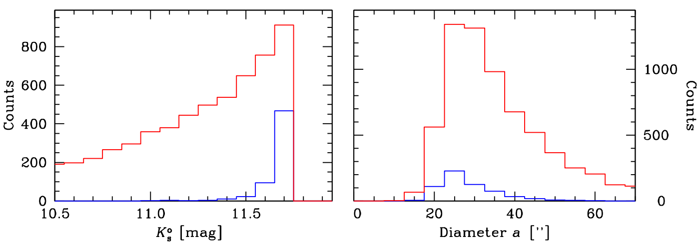

Fig. 9. Histograms of galaxies in the supplementary sample (S+, blue) as compared to the full sample (S, red). Left: As a function of extinction-corrected K_s band magnitude (with the diameter-dependent extinction correction applied for the S+ sample); right: as a function of diameter in arcseconds (also corrected for the S+ sample). The red histograms are truncated.

Finally, we present the mean and median colours for the various samples in Table 7. It is obvious that the colours become redder for the fainter samples, which is also the case for the high-latitude samples and thus not caused by the higher extinctions. Instead, such a shift is expected since we have not applied a k-correction. A similar shift has been noted for the bright sample in Paper II (see their Figure 8) where we compared (uncorrected) colours of galaxies in various redshift bins.

5.3. Extended sample

We have also derived a sample by applying a diameter-dependent extinction correction as explained above (and, in more detail, in Paper I). Since this is an additional correction, our sample is not complete anymore and we have to add those objects which have $K_s^o > 11\overset{m}{.}75$ but $K_s^{o,d} \leq 11\overset{m}{.}75$. The supplementary sample, labelled S+, comprises 1083 objects (see last entry in Table 5) and increases the galaxy sample by about 9%. The combined sample is called extended sample or S*e*.

The galaxies in the supplementary sample are faint, with a lower limit of $K_s^{o,d} = 11\overset{m}{.}00$ as shown in Fig. 9 in blue. For comparison, the full sample is shown in red. Note that we use the appropriately corrected K_s band magnitude for each sample. We also show the distribution with diameter, with a maximum diameter $a^d = 61''$ for S+.

The histograms over Galactic latitude, stellar densities and extinction are shown in Figures 10 and 11. Here we compare, on the one hand, the full sample S with the extended sample S*e* (in green and cyan, respectively), and, on the other hand, the two faint subsamples S3 and S3*e* with corrected magnitudes in the range $11\overset{m}{.}50 - 11\overset{m}{.}75$ (in magenta and black, respectively). For

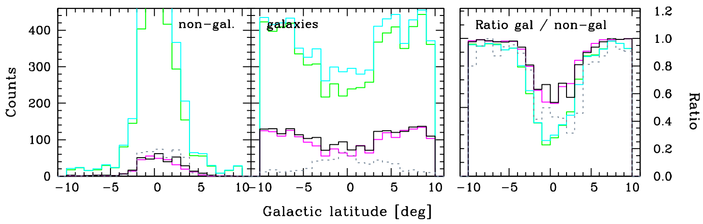

Fig. 10. Same as Fig. 6 for the full sample S (green), S*e* (cyan), S3 (magenta), S3*e* (the faint subsample of the extended sample; black) and S+ (dotted grey). The left-hand panel shows non-galaxies instead of all sources and is truncated to emphasise the comparison of the faint samples.

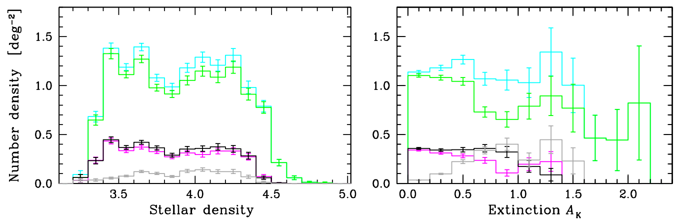

Fig. 11. Same as Fig. 8 for the full sample S (green), S*e* (cyan), S3 (magenta), S3*e* (the faint subsample of the extended sample; black) and S+ (dotted grey).

interest, we have added the S+ sample in dotted grey line. The differences between the two faint samples seems small, but the distribution of the S+ galaxies with a marked peak around the Galactic plane shows the importance of this sample for the completion rate. This is more pronounced in Fig. 11 where the S+ distribution with extinction shows a clear increase, resulting in the S3*e* sample to show a more even distribution with extinction than S3. We estimate the completion in the S*e* sample is about $A_K = 1\overset{m}{.}3$ and possibly up to $A_K = 1\overset{m}{.}5$. The distribution with stellar densities appears unaffected.

We added the statistics on the S+ sample to Table 6 though the total numbers of galaxies (587 and 18 in the ZOA and EBV samples, respectively) are small. Nonetheless, we can confirm that the trends with fainter samples hold for Disc class and velocities (with only 87 and 4 galaxies having a velocity measurement, respectively), while the extinction flags show a marked increase of almost a factor two for the ZOA sample.

Colours are largely unaffected by the additional diameter-dependent extinction correction[8], so we do not expect any qualitative differences in the mean or median. The change in sample size has only a negligible effect on the median values: we find 1.013 as compared to 1.011 for $(J - K_s)^{o,c}$ and 0.310 as compared to 0.309 for $(H - K_s)^{o,c}$.

6. Galactic extinction

In Paper II we have used the colours of the bright sample to investigate how well the extinction map used represents the line-of-sight Galactic extinction. We can now do the same using the full sample. In the following we distinguish between the already applied correction factor $f = 0.86$ and an additional factor f_a, which should be multiplied with f to arrive at a final value f_{new}. From the slope of the extinction-corrected $(J - K_s)^o$ colour–extinction relation for the full sample, we have thus derived $f_a = 0.98 \pm 0.01$, which confirms that the correction factor derived in Paper II is still acceptable. For simplicity, the following discussion will refer to f_a only.

In contrast to Paper II, we have excluded AGNs for this investigation (about 100 galaxies). While the effect on f_a is minimal (0.982 versus 0.981 with AGNs included), the intercept becomes slightly redder by $0\overset{m}{.}003$ (which if of the order of the error on the intercept) when AGNs are included, emphasising their redder colour.

In Paper II, we mention the effect of applying an upper limit in A_K on the slope of the fitted regression line. We have reinvestigated this and find a stable plateau for the the range $0\overset{m}{.}45 < \lim(A_K) \leq 1\overset{m}{.}1$ for the new sample. Including galaxies at higher extinctions introduces a bias due to on-sky variations in extinction smaller than the resolution of the extinction maps. We thus use $A_K = 1\overset{m}{.}1$ as the upper limit in our new investigation. Otherwise, we use the same selection criteria as in Paper II to ensure a photometrically clean sample.

As discussed in Sect. 5.2, the fainter galaxies in our new sample are often more distant, which may require a k-correction. We have done two tests: firstly, we derived f_a for the samples S1, S2 and S3 separately, see Table 8. We find that f_a slightly decreases with the fainter samples, indicating that the k-correction indeed becomes relevant. Figure 12 shows the redshift distribution of the various samples, confirming the shift towards higher redshifts for the fainter samples. As a second test we have selected only galaxies that have redshift information and compare how f_a changes when we apply the k-correction: The latter gives $f_a = 0.99 \pm 0.01$ as compared to $f_a = 0.98 \pm 0.01$ for the uncorrected ~ 4600 galaxies with redshift. The effect on the full sample is thus estimated negligible, though we should keep in mind a possible selection effect where predominantly brighter — and thus less distant — galaxies have been measured for redshift. Nonetheless, we expect the effect to be small, that is, less than the difference between the bright sample S1 and faint sample S3 ($\Delta f < 0.02$). In addition, we note that the intercept 1.00 ± 0.00 when using the k-correction is the same as the median $(J - K_s)$ colour for the high latitude bright sample (see Table 7).

We can now derive an improved 'map' of the f-values using bins in Galactic latitude and longitude. This will help to understand if there are intrinsic variations in the extinction properties across the Galactic plane. Since the binned samples will be much smaller than the full sample, we keep the intercept fixed to the value derived for the full sample and fit only the slope for each bin (see Sect. 5 in Paper II for details on the derivation). Figure 13 gives $\Delta f = f_{cell} - f_{all}$, with the small, $60° \times 5°$ cells in the top four rows, and larger, binned cells below (both in latitude, see, e.g., rows 5 – 7, and in longitude, see the bottom two panels). Contrary to Paper II, we use the neutral colour white for the range $-0.01 < \Delta f < 0.01$ (since 0.01 is the error on f_a in the unbinned sample). We do not apply the k-correction so as to maximise the number of galaxies in the individual bins and to avoid possible selection effects by uneven selection of galaxies that have or have not redshift measurements. We do need to keep in mind, though, a possible selection effect through large-scale structures that may lead to more distant galaxies in one bin and not in another.

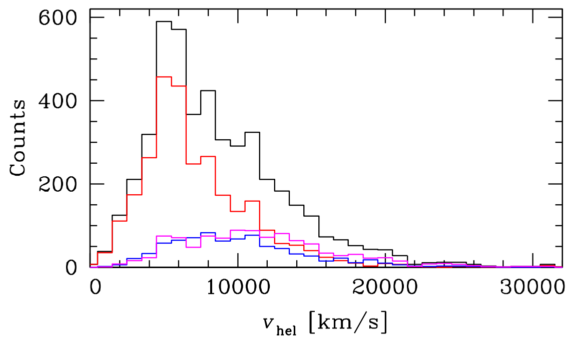

Fig. 12. Histogram of the redshift distribution of galaxies in the clean sample (black). The x-axis is truncated: there are six more galaxies between $v = 32000$ km s^{-1} and 56 360 km s^{-1}. Also shown are the histograms for the subsamples S1 (red), S2 (blue) and S3 (magenta).

Table 8. Object samples at different stages during extraction.

Sample	f_a	intercept	σ	N
Full sample	0.982 ± 0.007	1.034 ± 0.003	0.12	6155
S1	0.990 ± 0.009	1.026 ± 0.003	0.11	3178
S2	0.980 ± 0.015	1.037 ± 0.006	0.11	1189
S3	0.970 ± 0.014	1.045 ± 0.005	0.12	1788
Galaxies with velocity	0.978 ± 0.009	1.033 ± 0.003	0.10	4604
With k-correction	0.991 ± 0.009	0.996 ± 0.003	0.10	4604

b \ l	270° - 210°	210° - 150°	150° - 90°	90° - 30°	30° - 330°	330° - 270°
5° - 10°	-0.06:	0.04	0.01	0.04:	0.01	-0.06
0° - 5°	-0.04	0.00	0.01	0.01	0.00	-0.06
-5° - 0°	-0.02	0.03	0.01	-0.04	-0.04:	-0.04
-10° - -5°	-0.02	0.03	0.05	0.11:	0.07:	-0.15:
0° - 10°	-0.04	0.01	0.01	0.02	0.00	-0.06
-10° - 0°	-0.02	0.03	0.00	-0.02	0.03:	-0.06
-10° - 10°	-0.02	0.02	0.01	0.00	0.01	-0.06

b \ l		240° - 120°		60° - 300°	
5° - 10°		-0.00		-0.00	
0° - 5°		-0.00		-0.01	
-5° - 0°		0.01		-0.01:	
-10° - -5°		0.02		-0.05:	
0° - 10°		-0.00		-0.00	
-10° - 0°		0.01		-0.03:	
-10° - 10°		0.01		-0.01	

b \ l	... - 210°		150° - 30°		330° - ...°
5° - 10°	-0.06		0.01		
0° - 5°	-0.05		0.01		
-5° - 0°	-0.02		-0.00		
-10° - -5°	-0.06		0.07		
0° - 10°	-0.05		0.01		
-10° - 0°	-0.03		0.00		
-10° - 10°	-0.04		0.01		

-0.15/ -0.13	-0.12/ -0.10	-0.09/ -0.07	-0.06/ -0.04	-0.03/ -0.02	-0.01/ 0.01	0.02/ 0.03	0.04/ 0.06	0.07/ 0.09	0.10/ 0.12	0.13/ 0.15

Fig. 13. Binned sky map with Δf_a-values ($f_{cell} - f_{all}$) per cell. The colour scale is shown at the bottom. Red numbers may be overestimated, and colons indicate uncertain values. The 330° – 210° cells are wrapped around the Galactic Centre.

[8] Colours are derived using a fixed aperture across all bands, and in the outer parts of a galaxy the colour changes only little with a further increase of the diameter.

The map compares very well with the one for the bright sample (Fig. B4 in Paper II) with the exception of a stronger deviation in the range $210° < l < 330°$ which coincides with the direction of the dipole of the cosmic microwave background (CMB). However, no deviation is seen in the opposite direction. We need to keep in mind that overall the deviations shown in the map are mostly smaller than 3σ and thus not significant. Nonetheless, the negative Δf-values seen for those bins seem systematic and thus merit attention.

As a test, we have applied the *k*-correction, keeping in mind the above mentioned caveats. The systematics in the range $210° < l < 270°$ have disappeared and lessened in the adjacent direction $270° < l < 330°$, indicating that the deviation we see in Fig. 13 is likely due to selection effects through cosmic variance (note that both the Great Attractor as well as the Vela Supercluster are found in this direction).

7. Summary

We have presented the full 2MZoA catalogue with an extinction corrected magnitude limit of $K_s^o = 11\overset{m}{.}75$, covering the ZoA at latitudes $|b| < 10°$ (ZOA sample) and areas of high extinction ($E(B-V) > 0\overset{m}{.}950$; EBV sample) elsewhere. It thus serves as a complement to the 2MRS galaxy catalogue, resulting in the uniquely all-sky e2MRS survey. The catalogue comprises a total of 10 493 objects, of which 6899 are galaxies. Of the latter, 6757 are found in the ZOA sample, and 142 galaxies in the EBV sample. Compared to the catalogue of bright ($K_s^o \leq 11\overset{m}{.}25$) galaxies presented in Paper I, we have elected to use a different map of foreground extinction (the so-called GNILC extinction map by Planck Collaboration et al. 2016), with a correction factor $f = 0.86$ (see Paper II). We have also updated object classes (due to improved redshift and NIR information that have become available in the meantime), added a flag to identify quasars and active galaxies, revisited the extinction flag settings, and added redshift information.

We have discussed the properties of this new catalogue and have investigated possible differences to the bright sample ($K_s^o \leq 11\overset{m}{.}25$) due to the increased number of smaller and more distant galaxies. We have found that the fainter sample is less contaminated by non-galaxian objects like Galactic Nebulae. However, the fainter sample is more affected by Galactic foreground extinction and is, in contrast to the bright sample, not complete anymore even at low extinction levels. Stellar densities also seem to have an increased effect on the completion levels. We also find less redshift information in the literature for the fainter galaxies which, often due to high foreground extinction, are more difficult to observe spectroscopically. Based on the colours of the faintest galaxies ($11\overset{m}{.}50 < K_s^o \leq 11\overset{m}{.}75$), many of these are distant galaxies and would require a *k*-correction.

We have also compiled a supplementary sample of galaxies that become brighter than the magnitude cut when we apply an additional extinction-corrected diameter correction (see Paper I for details), resulting in 1083 additional objects, of which 587 are galaxies. The additional galaxies are predominantly found at high extinctions, improving the completion levels of the combined ('extended') sample for extinctions up to $A_K = 1\overset{m}{.}3$ and possibly beyond.

Finally, according to the recipe presented in Paper II, we have compiled a binned sky map of the correction factor f to be applied to the Galactic foreground extinction. Though we find larger deviations between cells than in Paper II, they are all within the 3σ errors, and the possible systematics found are likely due to cosmic variance. The full sample results in a correction factor $f_{new} = 0.84 \pm 0.01$, but due to the uncertainties in colours at the fainter end of our sample we continue to recommend the correction factor $f = 0.86 \pm 0.01$ as derived in Paper II.

The next steps in completing this project are as follows. (1) Improving the completion rate in the high stellar density area close to the Galactic Bulge could be achieved via by-eye searches and/or machine learning techniques (which might require additional by-eye verification, although the number of objects that needed visual inspection would be greatly reduced). Even more helpful would be searching the available deeper NIR images where the star crowding is alleviated through the higher spatial resolution of the images. Several galaxy catalogues extracted from the VVV and VVVX survey areas are already available (e.g., Alonso et al. 2025 and references therein). The drawback is that combining these catalogues with ours would lead to an inhomogeneously compiled 2MZoA catalogue which would need careful calibration and adjustments.

(2) An improvement of galaxy photometry is important for the cosmic flow field analysis. A semi-automated script that automatically subtracts stars and extracts galaxy photometry combined with a thorough by-eye quality control (e.g., Said 2017) would also remove some of the uncertainties in the magnitude limit of the sample.

(3) For completing the redshift survey, we need to obtain the missing redshifts. These would also help to improve the accuracy of the galaxy photometry via a consistent application of the *k*-correction for all galaxies. Redshift completeness can be achieved using the new generation of radio telescopes, the SKA and SKA precursors, for H I observations, and large ground based telescopes like SALT and HET or space telescopes like JWST for high quality IR of NIR spectroscopy.

Combined with the 2MRS, the here presented complementary catalogue forms the extended 2MRS survey, e2MRS, which comprises a nearly complete and homogeneous, magnitude-limited, all-sky galaxy catalogue. Apart from a small area (< 4% of the whole sky) in the direction of the Galactic Bulge, where galaxy detection is severely restricted by high stellar densities, e2MRS can be considered as unbiased. As such it is invaluable for studies of large-scale structures, flow fields and extinction across the whole sky including the ZoA.

Data availability

Tables A.1, A.2, A.3 and A.4 are available in electronic form at the CDS via anonymous ftp to cdsarc.u-strasbg.fr (130.79.128.5) or via http://cdsweb.u-strasbg.fr/cgi-bin/qcat?J/A+A/

Acknowledgements. The authors thank Lucas Macri for access to the most updated 2MRS data set. This research has made use of data products from the Two Micron All Sky Survey, which is a joint project of the University of Massachusetts and the Infrared Processing and Analysis Center, funded by the National Aeronautics and Space Administration and the National Science Foundation. This research also has made use of the HyperLeda database, the SIMBAD database, operated at CDS, Strasbourg, France, the NASA/IPAC Extragalactic Database (NED) which is operated by the Jet Propulsion Laboratory, California Institute of Technology, under contract with the National Aeronautics and Space Administration and the Digitized Sky Surveys which were produced at the Space Telescope Science Institute under U.S. Government grant NAG W-2166. This research has made use of the VizieR catalogue access tool, CDS, Strasbourg, France. The original description of the VizieR service was published in Ochsenbein et al. (2000). This research has made use of the Astrophysics Data System, funded by NASA under Cooperative Agreement 80NSSC25M7105.

References

Acker, A., Stenholm, B., & Veron, P. 1991, A&AS, 87, 499
Alam, S., Albareti, F. D., Allende Prieto, C., et al. 2015, ApJS, 219, 12
Alonso, M. V., Baravalle, L. D., Nilo-Castellón, J. L., et al. 2025, A&A, 700, A33
Beuing, J., Bender, R., Mendes de Oliveira, C., Thomas, D., & Maraston, C. 2002, A&A, 395, 431
Bicay, M. D. & Giovanelli, R. 1986a, AJ, 91, 705
Bicay, M. D. & Giovanelli, R. 1986b, AJ, 91, 732
Bicay, M. D. & Giovanelli, R. 1987, AJ, 93, 1326
Bilicki, M., Jarrett, T. H., Peacock, J. A., Cluver, M. E., & Steward, L. 2014, ApJS, 210, 9
Bottinelli, L., Durand, N., Fouque, P., et al. 1992, A&AS, 93, 173
Bottinelli, L., Durand, N., Fouque, P., et al. 1993, A&AS, 102, 57
Bottinelli, L., Gouguenheim, L., Loulergue, M., et al. 1994, in Astronomical Society of the Pacific Conference Series, Vol. 67, Unveiling Large-Scale Structures Behind the Milky Way, ed. C. Balkowski & R. C. Kraan-Korteweg, 225
Braun, R., Thilker, D., & Walterbos, R. A. M. 2003, A&A, 406, 829
Burton, W. B., Verheijen, M. A. W., Kraan-Korteweg, R. C., & Henning, P. A. 1996, A&A, 309, 687
Chamaraux, P., Cayatte, V., Balkowski, C., & Fontanelli, P. 1990, A&A, 229, 340
Chamaraux, P., Kazes, I., Saito, M., Yamada, T., & Takata, T. 1995, A&A, 299, 347
Chamaraux, P., Masnou, J.-L., Kazés, I., et al. 1999, MNRAS, 307, 236
Collobert, M., Sarzi, M., Davies, R. L., Kuntschner, H., & Colless, M. 2006, MNRAS, 370, 1213
Corwin, Jr., H. G. & Emerson, D. 1982, MNRAS, 200, 621
Cote, S., Freeman, K. C., Carignan, C., & Quinn, P. J. 1997, AJ, 114, 1313
Courtois, H. M., Tully, R. B., Fisher, J. R., et al. 2009, AJ, 138, 1938
Courtois, H. M., Tully, R. B., Makarov, D. I., et al. 2011, MNRAS, 414, 2005
Crawford, C. S., Edge, A. C., Fabian, A. C., et al. 1995, MNRAS, 274, 75
Crook, A. C., Huchra, J. P., Martimbeau, N., et al. 2007, ApJ, 655, 790
Davies, R. D., Staveley-Smith, L., & Murray, J. D. 1989, MNRAS, 236, 171
Davies, R. L., Burstein, D., Dressler, A., et al. 1987, ApJS, 64, 581
Davoust, E. & Considere, S. 1995, A&AS, 110, 19
Daza-Perilla, I. V., Sgró, M. A., Baravalle, L. D., et al. 2023, MNRAS, 524, 678
di Nella, H., Couch, W. J., Parker, Q. A., & Paturel, G. 1997, MNRAS, 287, 472
di Nella, H., Paturel, G., Walsh, A. J., et al. 1996, A&AS, 118, 311
Djorgovski, S., Thompson, D. J., de Carvalho, R. R., & Mould, J. R. 1990, AJ, 100, 599
Donley, J. L., Koribalski, B. S., Staveley-Smith, L., et al. 2006, MNRAS, 369, 1741
Donley, J. L., Staveley-Smith, L., Kraan-Korteweg, R. C., et al. 2005, AJ, 129, 220
Dressler, A. 1991, ApJS, 75, 241
Dressler, A., Lynden-Bell, D., Burstein, D., et al. 1987, ApJ, 313, 42
Dupuy, A., Courtois, H. M., Guinet, D., Tully, R. B., & Kourkchi, E. 2021, A&A, 646, A113
Durret, F., Wakamatsu, K., Nagayama, T., Adami, C., & Biviano, A. 2015, A&A, 583, A124
Dutra, C. M., Ahumada, A. V., Clariá, J. J., Bica, E., & Barbuy, B. 2003, A&A, 408, 287
Dye, S., Lawrence, A., Read, M. A., et al. 2018, MNRAS, 473, 5113
Ebeling, H., Mullis, C. R., & Tully, R. B. 2002, ApJ, 580, 774
Eracleous, M. & Halpern, J. P. 2004, ApJS, 150, 181
Fairall, A. P. 1983, MNRAS, 203, 47
Fairall, A. P. 1988a, MNRAS, 230, 69
Fairall, A. P. 1988b, MNRAS, 233, 691
Fairall, A. P., Vettolani, G., & Chincarini, G. 1989, A&AS, 78, 269
Fairall, A. P. & Woudt, P. A. 2006, MNRAS, 366, 267
Fairall, A. P., Woudt, P. A., & Kraan-Korteweg, R. C. 1998, A&AS, 127, 463
Falco, E. E., Kurtz, M. J., Geller, M. J., et al. 1999, PASP, 111, 438
Fisher, K. B., Huchra, J. P., Strauss, M. A., et al. 1995, ApJS, 100, 69
Fitzpatrick, E. L. 1999, PASP, 111, 63
Focardi, P., Marano, B., & Vettolani, G. 1984, A&A, 136, 178
Freeman, K. C., Karlsson, B., Lynga, G., et al. 1977, A&A, 55, 445
Freudling, W. 1995, A&AS, 112, 429
Fuerst, E., Reich, W., Kuehr, H., & Stickel, M. 1989, A&A, 223, 66
Giovanelli, R. & Haynes, M. P. 1981, AJ, 86, 340
Giovanelli, R. & Haynes, M. P. 1982, AJ, 87, 1355
Golovich, N., van Weeren, R. J., Dawson, W. A., Jee, M. J., & Wittman, D. 2017, ApJ, 838, 110
Gordon, D. & Gottesman, S. T. 1981, AJ, 86, 161
Hasegawa, T., Wakamatsu, K.-i., Malkan, M., et al. 2000, MNRAS, 316, 326
Hauschildt, M. 1987, A&A, 184, 43
Haynes, M. P., Giovanelli, R., Herter, T., et al. 1997, AJ, 113, 1197
Haynes, M. P., Giovanelli, R., Kent, B. R., et al. 2018, ApJ, 861, 49
Henning, P. A., Springob, C. M., Minchin, R. F., et al. 2010, AJ, 139, 2130
Hong, T., Staveley-Smith, L., Masters, K. L., et al. 2013, MNRAS, 432, 1178
Huchra, J. P., Geller, M. J., Clemens, C. M., Tokarz, S. P., & Michel, A. 1992, Bulletin d'Information du Centre de Donnees Stellaires, 41, 31
Huchra, J. P., Macri, L. M., Masters, K. L., et al. 2012, ApJS, 199, 26
Huchtmeier, W. K., Karachentsev, I. D., & Karachentseva, V. E. 2001, A&A, 377, 801
Huchtmeier, W. K., Karachentsev, I. D., & Karachentseva, V. E. 2003, A&A, 401, 483
Huchtmeier, W. K., Karachentsev, I. D., Karachentseva, V. E., & Ehle, M. 2000, A&AS, 141, 469
Huchtmeier, W. K., Karachentsev, I. D., Karachentseva, V. E., Kudrya, Y. N., & Mitronova, S. N. 2005, A&A, 435, 459
Huchtmeier, W. K., Lercher, G., Seeberger, R., Saurer, W., & Weinberger, R. 1995, A&A, 293, L33
Hudson, M. J., Smith, R. J., Lucey, J. R., & Branchini, E. 2004, MNRAS, 352, 61
Hunstead, R. W., Murdoch, H. S., & Shobbrook, R. R. 1978, MNRAS, 185, 149
Im, M., Lee, I., Cho, Y., et al. 2007, ApJ, 664, 64
Iwata, I. & Chamaraux, P. 2011, A&A, 531, A87
Jarrett, T. H. 2004, Publications of the Astronomical Society of Australia, 21, 396
Jarrett, T. H., Chester, T., Cutri, R., et al. 2000, AJ, 120, 298
Jarrett, T. H., Cohen, M., et al. 2011, ApJ, 735, 112
Jones, D. H., Read, M. A., Saunders, W., et al. 2009, MNRAS, 399, 683
Jones, D. H., Saunders, W., Read, M., & Colless, M. 2005, PASA, 22, 277
Jones, P. A. & McAdam, W. B. 1992, ApJS, 80, 137
Kobulnicky, H. A., Dickey, J. M., Sargent, A. I., Hogg, D. E., & Conti, P. S. 1995, AJ, 110, 116
Koss, M. J., Ricci, C., Trakhtenbrot, B., et al. 2022a, ApJS, 261, 2
Koss, M. J., Trakhtenbrot, B., Ricci, C., et al. 2022b, ApJS, 261, 6
Kourkchi, E. & Tully, R. B. 2017, ApJ, 843, 16
Kraan-Korteweg, R. C., Cluver, M. E., Bilicki, M., et al. 2017, MNRAS, 466, L29
Kraan-Korteweg, R. C., Fairall, A. P., & Balkowski, C. 1995, A&A, 297, 617
Kraan-Korteweg, R. C., Henning, P. A., & Schröder, A. C. 2002, A&A, 391, 887
Kraan-Korteweg, R. C. & Huchtmeier, W. K. 1992, A&A, 266, 150
Kraan-Korteweg, R. C. & Lahav, O. 2000, A&Ar, 10, 211
Kraan-Korteweg, R. C., van Driel, W., Schröder, A. C., Ramatsoku, M., & Henning, P. A. 2018, MNRAS, 481, 1262
Kraan-Korteweg, R. C., Woudt, P. A., Cayatte, V., et al. 1996, Nature, 379, 519
Kregel, M., van der Kruit, P. C., & de Blok, W. J. G. 2004, MNRAS, 352, 768
Lahav, O., Brosch, N., Goldberg, E., et al. 1998, MNRAS, 299, 24
Lang, R. H., Boyce, P. J., Kilborn, V. A., et al. 2003, MNRAS, 342, 738
Lara, L., Márquez, I., Cotton, W. D., et al. 2001, A&A, 378, 826
Lavaux, G. & Hudson, M. J. 2011, MNRAS, 416, 2840
Lawrence, A., Rowan-Robinson, M., Ellis, R. S., et al. 1999, MNRAS, 308, 897

Ledlow, M. J., Owen, F. N., & Miller, N. A. 2005, AJ, 130, 47
Lewis, B. M., Helou, G., & Salpeter, E. E. 1985, ApJS, 59, 161
Liu, X.-W., Zhao, G., & Hou, J.-L. 2015, Research in Astronomy and Astrophysics, 15, 1089
Lu, N. Y., Dow, M. W., Houck, J. R., Salpeter, E. E., & Lewis, B. M. 1990, ApJ, 357, 388
Lu, N. Y. & Freudling, W. 1995, ApJ, 449, 527
Lucas, P. W., Hoare, M. G., Longmore, A., et al. 2008, MNRAS, 391, 136
Macri, L. M., Kraan-Korteweg, R. C., Lambert, T., et al. 2019, ApJS, 245, 6
Martin, J. M., Bottinelli, L., Dennefeld, M., et al. 1990, A&A, 235, 41
Martin, J. M., Bottinelli, L., Dennefeld, M., & Gouguenheim, L. 1991, A&A, 245, 393
Marzke, R. O., Huchra, J. P., & Geller, M. J. 1996, AJ, 112, 1803
Masetti, N., Mason, E., Morelli, L., et al. 2008, A&A, 482, 113
Masetti, N., Parisi, P., Palazzi, E., et al. 2010, A&A, 519, A96
Masters, K. L., Crook, A., Hong, T., et al. 2014, MNRAS, 443, 1044
Mathewson, D. S. & Ford, V. L. 1996, ApJS, 107, 97
McIntyre, T. P., Henning, P. A., Minchin, R. F., Momjian, E., & Butcher, Z. 2015, AJ, 150, 28
Meyer, M. J., Zwaan, M. A., Webster, R. L., et al. 2004, MNRAS, 350, 1195
Minniti, D., Lucas, P. W., Emerson, J. P., et al. 2010, New Astronomy, 15, 433
Mitronova, S. N., Huchtmeier, W. K., Karachentsev, I. D., Karachentseva, V. E., & Kudrya, Y. N. 2005, Astronomy Letters, 31, 501
Monnier Ragaigne, D., van Driel, W., O'Neil, K., et al. 2003, A&A, 408, 67
Morganti, R., Emonts, B., & Oosterloo, T. 2009, A&A, 496, L9
Motch, C., Guillout, P., Haberl, F., et al. 1998, A&AS, 132, 341
Nakanishi, K., Takata, T., Yamada, T., et al. 1997, ApJS, 112, 245
Nilsson, K., Pursimo, T., Heidt, J., et al. 2003, A&A, 400, 95
Ochsenbein, F., Bauer, P., & Marcout, J. 2000, A&AS, 143, 23
Ogando, R. L. C., Maia, M. A. G., Pellegrini, P. S., & da Costa, L. N. 2008, AJ, 135, 2424
Owen, F. N., Ledlow, M. J., Morrison, G. E., & Hill, J. M. 1997, ApJ, 488, L15
Pantoja, C. A., Altschuler, D. R., Giovanardi, C., & Giovanelli, R. 1997, AJ, 113, 905
Pantoja, C. A., Giovanardi, C., Altschuler, D. R., & Giovanelli, R. 1994, AJ, 108, 921
Paturel, G., Theureau, G., Bottinelli, L., et al. 2003, A&A, 412, 57
Pesce, D. W., Braatz, J. A., Condon, J. J., & Greene, J. E. 2018, ApJ, 863, 149
Planck Collaboration, Aghanim, N., Ashdown, M., et al. 2016, A&A, 596, A109
Proust, D., Mazure, A., Vanderriest, C., Sodre, Jr., L., & Capelato, H. V. 1995, A&AS, 114, 565
Radburn-Smith, D. J., Lucey, J. R., Woudt, P. A., Kraan-Korteweg, R. C., & Watson, F. G. 2006, MNRAS, 369, 1131
Ramatsoku, M., Verheijen, M. A. W., Kraan-Korteweg, R. C., et al. 2016, MNRAS, 460, 923
Riad, I. F., Kraan-Korteweg, R. C., & Woudt, P. A. 2010, MNRAS, 401, 924
Roman, A. T., Takeuchi, T. T., Nakanishi, K., & Saito, M. 1998, PASJ, 50, 47
Rosenberg, J. L. & Schneider, S. E. 2000, ApJS, 130, 177
Sadler, E. M. 1984, AJ, 89, 23
Said K., 2017, PhD thesis, University of Cape Town
Said, K., Kraan-Korteweg, R. C., Staveley-Smith, L., et al. 2016, MNRAS, 457, 2366
Saito, R. K., Hempel, M., Alonso-García, J., et al. 2024, A&A, 689, A148
Sanchez-Barrantes, M., Henning, P. A., McIntyre, T., et al. 2019, AJ, 158, 234
Sandage, A. 1976, PASP, 88, 367
Sanders, D. B., Egami, E., Lipari, S., Mirabel, I. F., & Soifer, B. T. 1995, AJ, 110, 1993
Sargent, W. L. W. 1973, ApJ, 182, L13
Saunders, W., Sutherland, W. J., Maddox, S. J., et al. 2000, MNRAS, 317, 55
Schlafly, E. F., Green, G. M., Lang, D., et al. 2018, ApJS, 234, 39
Schlegel, D. J., Finkbeiner, D. P., & Davis, M. 1998, ApJ, 500, 525
Schneider, S. E., Thuan, T. X., Mangum, J. G., & Miller, J. 1992, ApJS, 81, 5
Schröder, A. C., Flöer, L., Winkel, B., & Kerp, J. 2019, MNRAS, 489, 2907
Schröder, A. C., Kraan-Korteweg, R. C., & Henning, P. A. 2009, A&A, 505, 1049
Schröder, A. C., van Driel, W., & Kraan-Korteweg, R. C. 2021, MNRAS, 503, 5351
Schröder, A. C., van Driel, W., Kraan-Korteweg, R. C., & Belleval, C. 2025, A&A, 695, A79
Seeberger, R., Huchtmeier, W. K., & Weinberger, R. 1994, A&A, 286, 17
Seeberger, R. & Saurer, W. 1998, A&AS, 127, 101
Sekiguchi, K. & Wolstencroft, R. D. 1992, MNRAS, 255, 581
Skrutskie, M. F., Cutri, R. M., Stiening, R., et al. 2006, AJ, 131, 1163
Spinrad, H. 1975, ApJ, 199, L1
Springob, C. M., Haynes, M. P., Giovanelli, R., & Kent, B. R. 2005, ApJS, 160, 149
Springob, C. M., Hong, T., Staveley-Smith, L., et al. 2016, MNRAS, 456, 1886
Staveley-Smith, L., Kraan-Korteweg, R. C., Schröder, A. C., et al. 2016, AJ, 151, 52
Strauss, M. A., Huchra, J. P., Davis, M., et al. 1992, ApJS, 83, 29
Sulentic, J. W. & Arp, H. 1983, AJ, 88, 489
Takata, T., Yamada, T., Saito, M., Chamaraux, P., & Kazes, I. 1994, A&AS, 104, 529
Theureau, G., Bottinelli, L., Coudreau-Durand, N., et al. 1998, A&AS, 130, 333
Theureau, G., Coudreau, N., Hallet, N., et al. 2005, A&A, 430, 373
Theureau, G., Coudreau, N., Hallet, N., Hanski, M. O., & Poulain, M. 2017, A&A, 599, A104
Theureau, G., Hanski, M. O., Coudreau, N., Hallet, N., & Martin, J. M. 2007, A&A, 465, 71
Tifft, W. G. & Cocke, W. J. 1988, ApJS, 67, 1
Tully, R. B., Pomarède, D., Graziani, R., et al. 2019, ApJ, 880, 24
Tully, R. B. et al. 2008, ApJ, 676, 184
van den Bosch, R. C. E., Gebhardt, K., Gültekin, K., Yıldırım, A., & Walsh, J. L. 2015, ApJS, 218, 10
Visvanathan, N. & van den Bergh, S. 1992, AJ, 103, 1057
Visvanathan, N. & Yamada, T. 1996, ApJS, 107, 521
Wegner, G., Bernardi, M., Willmer, C. N. A., et al. 2003, AJ, 126, 2268
West, R. M., Surdej, J., Schuster, H. E., et al. 1981, A&AS, 46, 57
West, R. M. & Tarenghi, M. 1989, A&A, 223, 61
Wong, O. I., Ryan-Weber, E. V., Garcia-Appadoo, D. A., et al. 2006, MNRAS, 371, 1855
Woudt, P. A., Kraan-Korteweg, R. C., Cayatte, V., Balkowski, C., & Felenbok, P. 2004, A&A, 415, 9
Woudt, P. A., Kraan-Korteweg, R. C., & Fairall, A. P. 1999, A&A, 352, 39
Woudt, P. A., Kraan-Korteweg, R. C., Lucey, J., Fairall, A. P., & Moore, S. A. W. 2008, MNRAS, 383, 445
Wouterloot, J. G. A. & Brand, J. 1989, A&AS, 80, 149
Yamada, T. & Saito, M. 1993, PASJ, 45, 25
Yamada, T., Tomita, A., Saito, M., Chamaraux, P., & Kazes, I. 1994, MNRAS, 270, 93
Zirbel, E. L. & Baum, S. A. 1995, ApJ, 448, 521
Zurita Heras, J. A., Chaty, S., & Tomsick, J. A. 2009, A&A, 502, 787

Appendix A: Tables

The four tables A.1 – A.4 are available electronically at the CDS. For clarity, we list in this section some example lines for each table.

Table A.1 presents the full catalogue. The columns are described in Sect. 3.

For the radial velocity information in Table A.1, we searched the literature for our objects. We were mainly interested in original measurements and do not list all available compilations. We searched online databases (NED, Simbad, Leda) as well as catalogues available at the CDS. Though we concentrated on objects classified as galaxies, we also searched systematically for object class 5 (unknown) and 6 (lower likelihood for being a galaxy) to be comprehensive.

The compilation of the velocities is given in Table A.2 for optical velocities, and in Table A.3 for H I measurements. The tables give one line per velocity and reference per object. They are ordered by (a) error (or quality) for original measurements, (b) re-reductions (unless superseding the original publication), (c) by publication year for referenced values (indicated by 'c'; in Col. 2), and (d) averaged values or non-detection entries. Non-accepted values (for example detection of another galaxy nearby or wrong measurements) are marked in the flag column.

The columns in the two tables are as follows:

- Col. 1: ID: 2MASX catalogue identification number (based on J2000.0 coordinates).
- Cols. 2 – 5: Flags repeated from Cols 9, 4, 5 and 6 from Table A.1.
- Col. 6: Velocity measurement flags refering to the quoted publication. They are similar to the flags in Col. 10 of Table A.1 with the addition of 'c' for compilation, 'a' for compilation that gives averaged values, 'r' for re-reduced, and 'n' for non detections.
- Cols. 7 – 9: Redshift value and error in kilometre per second and the bibcode of the reference (see Table A.4 for details).
- Col. 10: Comments. An arrow indicates a quoted reference (usually also listed by us in this table), single quotes refer to comments made in the publication. Where possible we give telescope or instrument information (see also Table A.4 for generic information regarding the publication).

Table A.4 lists the references used in Tables A.2 and A.3 with: (1) Bibcode; (2) Name of first author; (3) Source of data (either the wavelength regime or literature); (4) Observational and velocity information where relevant (e.g., telescope used, precision of the velocity); (5) Comments.

Appendix B: Sky maps

The on-sky distribution of both the ZOA and the EBV samples is shown in Fig. B.1, with galaxies shown in grey and non-galaxies in yellow. Magenta dots show galaxies from the extended sample (that is, with a diameter-dependent extinction correction applied). There are only a few areas at higher latitudes ($b \geq 10°$) that have extinctions high enough to be in the EBV sample.

Table A.1. 2MZoA sample Part I (example lines).

2MASX J	l	b	EBV		Object			Sample	Disc	2MRS		Vel flag		NIR	Phot	Ext
	deg	deg	mag	cl	off	obj	g	sobnei	type		Op	HI	Tot			
(1)	(2a)	(2b)	(3)	(4)	(5)	(6)		(7)	(8)	(9)		(10)		(11)	(12)	(13)
00000637+5319136	115.217	-8.780	0.303	1	-	-	g	111111	D4	c	o	-	o	H	-	-
00093966+5301008	116.587	-9.339	0.390	1	-	-	g	100110	D2	cp	-	-	-	H	P	e?
01475111+6305278	129.264	0.915	1.452	9	e	-	-	111111	-	-	-	-	-	-	OC	-
03044401+5406473	141.761	-3.812	1.006	1	-	-	g	111111	D1	e	o	[h?]	o	U	-	-
03382146+6419229	139.827	7.075	0.811	1	-	-	g	100110	D1	c	o	-	o	-	-	-
05434399+1637482	190.314	-6.764	0.397	1	-	-	g	100110	D1	c	o	h	h	H	-	-
06102125+1642343	193.430	-1.196	2.358	7	-	-	-	111111	-	-	-	-	-	U	-	-
06553807-0705580	219.730	-2.303	0.982	1	-	-	g	100110	D1	-	-	h:	h:	U	-	-
07561963-4137420	256.656	-6.723	0.799	1	-	q	g	111111	D1	c	o	-	o	-	-	e?
08210735-4321103	260.583	-3.796	2.319	1	-	-	g	110111	D1	-	-	-	-	V	-	e

Table A.1. 2MZoA sample Part II (example lines).

K_{20}	H-K	J-K	vc	a	b/a	st.d.	K_s^o	$(H\text{-}K)^o$	$(J\text{-}K)^o$	A_K	a^d	$K_s^{o,d}$	vel		Reference
mag	mag	mag		"			mag	mag	mag	mag	″	mag	km s^{-1}		
(14)	(15)	(16)	(17)	(18)	(19)	(20)	(21)	(22)	(23)	(24)	(25)	(26)	(27)		(28)
11.196	0.42	1.15	1	35.0	0.62	3.59	11.102	0.38	1.02	0.09	35.6	11.09	12447	65	2012ApJS..199...26H
11.635	0.37	1.23	1	32.4	0.68	3.46	11.514	0.31	1.06	0.12	33.2	11.50	—	–	—
11.382	0.60	1.54	-2	104.8	0.44	3.85	10.932	0.39	0.91	0.45	126.5	10.73	—	–	—
8.750	0.44	1.46	1	120.6	0.76	3.59	8.438	0.29	1.02	0.31	128.8	8.41	2467	29	2015ApJS..218...10V
11.920	0.54	1.54	1	24.8	0.48	3.56	11.669	0.42	1.19	0.25	26.5	11.63	11272	300	1999MNRAS.308..897L
11.502	0.39	1.37	1	46.4	0.24	3.47	11.379	0.33	1.20	0.12	47.6	11.36	8888	12	2017A&A...599A.104T
11.794	1.50	3.23	1	18.0	0.84	3.70	11.064	1.15	2.22	0.73	23.0	10.91	—	–	—
11.955	0.39	1.35	1	23.0	0.44	3.69	11.651	0.24	0.92	0.30	25.0	11.60	5571	20	2005A&A...430..373T
10.247	0.53	1.44	1	42.6	0.72	3.69	9.999	0.41	1.09	0.25	44.8	9.98	6558	17	2022ApJS..261....6K
12.016	0.72	1.87	1	30.4	0.78	3.86	11.298	0.38	0.87	0.72	40.9	11.04	—	–	—

Table A.2. Optical velocity information (example lines).

2MASXJ ID	2MRS		Object		fl_{vel}	Vel	err	Reference	Comment
		cl	off	obj					
00000637+5319136	c	1	-	-	o	12447	65	2012ApJS..199...26H	L
01345288+5524083	c	1	-	-	o	5765	50	1999PASP..111..438F	('unpublished FAST observation'); H(err=5)
01345288+5524083	c	1	-	-	o?	[7643	22	1999ApJS..121..287H]	(wrong match in NED, see 2MASXJ01343978+5525029)
04472448+4854366	-	1	-	-	o	3031	50	1994A&AS..104..529T	
04472448+4854366	-	1	-	-	c	3031		2000MNRAS.317...55S	-> T94
08294860-2208039	c	1	-	-	o:	6350	100	1994MNRAS.270...93Y	('uncertain'; NED: err=20); H
08294860-2208039	c	1	-	-	c	6350		1993ApJS...89...57Y	-> Y94
08294860-2208039	c	1	-	-	c	6350		1996ApJS..107..521V	-> Y94
08294860-2208039	c	1	-	-	c	6350		2000MNRAS.317...55S	-> Y94
21273973+4528586	e	1	-	-	o	5265		2001AJ....122.2381M	(Kitt Peak)
21273973+4528586	e	1	-	-	c	5265		2001AJ....122.2396D	-> M01

Table A.3. H I velocity information (example lines).

2MASXJ ID	2MRS		Object		fl_{vel}	Vel	err	Reference	Comment
		cl	off	obj					
00265906+6049388	-	1	-	-	h	7101	8	2018MNRAS.481.1262K	('marg')
00384223+6017130	-	1	-	-	h	4354	5	2018MNRAS.481.1262K	
00384223+6017130	-	1	-	-	h	4355		1992ApJS...78..365H	(noisy profile)
00384223+6017130	-	1	-	-	h:	4300		1987ApJ...320L..99K	
00384223+6017130	-	1	-	-	c	4355	22	1992BICDS..41...31H	-> H92
00414439+5309441	c	1	-	-	n	[9717		2021A&A...646A.113D]	('not detected')
02550583+6624065	e	1	-	-	h	3485		2009AJ....138.1938C	(GBT; err 6)
04395830+4920510	e	1	-	-	h	-9999	7	2018ZOATF.NRT.0000K	('confused')
14300299-5234205	c	1	o	-	h?	4513		2004MNRAS.350.1195M	(err=9; possible cross-match)
14300299-5234205	c	1	o	-	r?	4508		2005MNRAS.361...34D	
22420452+5108042	c	1	-	-	m:	8017	15	1994A&A...286...17S	('marg', snr=2.0); HL

Table A.4. References for the redshifts (examples).

Bibcode	First author	Source	Obs/vel information	Comments
1967AJ.....72..821P	Page	opt	v_corr	
1980Ap.....16..353M	Markarian	opt	SAO; z 4-digit	not systematical (no coordinates given); = 1980Afz....16..353M
1982ApJ...255..373G	Gregory	opt	v_galactocentric	converted in Leda
1991srcp.book.....F	Fairall	lit	mostly averaged	
1992ApJS...83...29S	Strauss	opt, lit		references -5xx and -1 are observations, others see ZCAT
1999MNRAS.308..897L	Lawrence	opt, lit	WHT	QDOT; reference IDs see 2000MNRAS.317...55S
2004MNRAS.350.1195M	Meyer	HI	PKS, vres=26	blind survey; HIPASS; err from NED; = 2006HIPAS.C...0000: on NED
2018MNRAS.481.1262K	Kraan-Korteweg	HI	NRT, vres=18	
2022ApJS..261....2K	Koss	opt, lit	z 8-digit	BASS-DR2; -> DR1

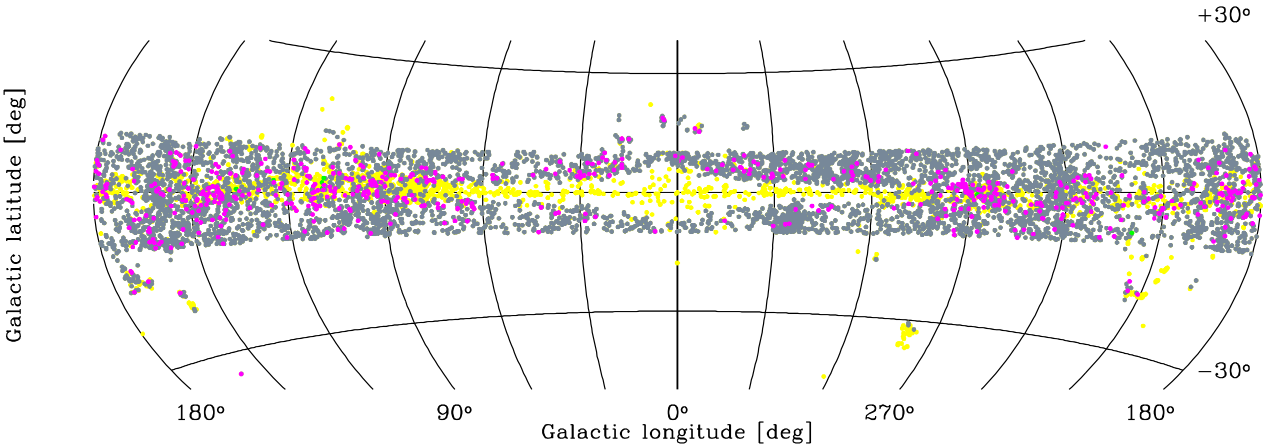

Fig. B.1. Aitoff projection in Galactic coordinates of the ZOA and EBV samples. Grey dots are galaxies, yellow dots non-galaxies, and green dots objects of unknown nature. Magenta dots indicate galaxies that are added through the diameter-depended extinction correction.